Annales
Geophysicae

The response of the H geocorona between 3 and 8 R_e to geomagnetic disturbances studied using TWINS stereo Lyman-α data

Jochen H. Zoennchen[1], Uwe Nass[1], Hans J. Fahr[1], and Jerry Goldstein[2,3]

[1]Argelander Institut für Astronomie, Astrophysics Department, University of Bonn, Auf dem Huegel 71,
53121 Bonn, Germany
[2]Southwest Research Institute, San Antonio, Texas, USA
[3]University of Texas, San Antonio, San Antonio, Texas, USA

Correspondence to: Jochen H. Zoennchen (zoenn@astro.uni-bonn.de)

Abstract. Circumterrestrial Lyman-α column brightness observations from 3–8 Earth radii (R_e) have been used to study temporal density variations in the exospheric neutral hydrogen as response to geomagnetic disturbances of different strength, i.e., Dst peak values between -26 and -147 nT. The data used were measured by the two Lyman-α detectors (LAD1/2) onboard both TWINS satellites between the solar minimum of 2008 and near the solar maximum of 2013. The solar Lyman-α flux at 121.6 nm is resonantly scattered near line center by exospheric H atoms and measured by the TWINS LADs. Along a line of sight (LOS), the scattered LOS-column intensity is proportional to the LOS H column density, assuming optically thin conditions above 3 R_e. In the case of the eight analyzed geomagnetic storms we found a significant increase in the exospheric Lyman-α flux between 9 and 23 % (equal to the same increase in H column density Δn_H) compared to the undisturbed case short before the storm event. Even weak geomagnetic storms (e.g., Dst peak values ≥ -41 nT) under solar minimum conditions show increases up to 23 % of the exospheric H densities. The strong H density increase in the observed outer exosphere is also a sign of an enhanced H escape flux during storms. For the majority of the storms we found an average time shift of about 11 h between the time when the first significant dynamic solar wind pressure peak (p_{SW}) hits the Earth and the time when the exospheric Lyman-α flux variation reaches its maximum. The results show that the (relative) exospheric density reaction of Δn_H have a tendency to decrease with increasing peak values of Dst index or the Kp index daily sum. Nevertheless, a simple linear correlation between Δn_H and these two geomagnetic indices does not seem to exist. In contrast, when recovering from the peak back to the undisturbed case, the Kp index daily sum and the Δn_H essentially show the same temporal recovery.

1 Introduction

The main component of the terrestrial exosphere are neutral hydrogen atoms, in particular in the analyzed regions with geocentric distances between 3 and 8 Earth radii (R_e).

Besides the study of corresponding exospheric H density distributions to various (but stable) solar activity level (or seasonal configurations), the analysis of short time H density variations as a direct exospheric response to geomagnetic storms contains ample information of the exosphere's nature, e.g., about different transport processes initially triggered by sudden solar wind variations hitting the Earth.

Since the geocoronal H atoms produce a Lyman-α glow by resonant scattering of solar Lyman-α radiation at 121.6 nm, the observation of geocoronal Lyman-α column brightness and its conversion into exospheric H density models have challenged researchers for decades. In the past, observations have been carried out with high-altitude rockets or satellites (e.g., Kupperian et al., 1959; Johnson, 1961; Rairden et al., 1986; Østgaard et al., 2003) and even by Apollo 16 from the Moon (Carruthers et al., 1976). Numerous theoretical studies on this subject have been published (e.g., Chamberlain, 1963;

Thomas and Bohlin, 1972; Fahr and Shizgal, 1983; Bishop, 1991; Hodges Jr., 1994).

Onboard the two TWINS (Two Wide-angle Imaging Neutral-atom Spectrometers) satellites (McComas et al., 2009). The Lyman-α detectors (LADs) have provided nearly continuous, circumterrestrial Lyman-α monitoring of the exosphere (from geocentric distances between ≈ 4.5 and 7.2 R_e) since 2008.

Based on TWINS-LAD data Bailey and Gruntman (2013) reported a H density increase for several geomagnetic storms in 2011 by comparing 3-D density fits of the H geocorona near the storm's maximum with the undisturbed case. From their analysis they derived an linear correlation between the peak Dst index of the storm and the relative variation in the exospheric H density, which also predicts nearly no exospheric reaction for weak storms with peak values of Dst index > -50 nT. From the results of this work here, however, we can not confirm this correlation.

In the present study we used a different analytic approach to study the exospheric H column density variation. Instead of a H density model fit we compared pairs of geometrically similar LOS observations taken with time shift intervals of approximately 24 h. In addition, we consider a broader range of the Dst index peak values between -25 and -145 nT as well as different solar activity conditions in this study. Therefore we have analyzed eight different geomagnetic storms, observed under solar minimum and solar maximum conditions between 2008 and 2013. Interestingly, we found that very weak storms (peak values of Dst index > -41 nT) under solar minimum in 2008 also cause significant H column density variations (up to 23 %). These storms are best covered with TWINS LAD in terms of spatial and temporal resolution since simultaneously observed LAD data of both TWINS satellites are available from this period.

2 TWINS Lyman-α detectors and mission performance

Since the middle of 2008 the TWINS 1 and 2 satellites have been operating at high-elliptic Molniya orbits around the Earth (apogee ≈ 7.2 R_e). As soon as they are at geocentric distances above 4.5 R_e (in the Northern Hemisphere) the LADs are activated for observation with the view directions always facing south (see details in Nass et al., 2006). There is an angular shift of the apogee positions of about 35° between TWINS 1 and 2. The two LADs per TWINS satellite observe the H geocorona under a tilt angle of 40° (field of view 4°) with respect to the Earth. They are mounted on a 180° forward- and backward-rotating actuator, which allows for the observation of a full circle (band of 4° width) on the sky after ≈ 90 s. The time between two individual LAD observations is 0.67 s.

On a longer timescale (e.g., months) the LADs' sensitivity continuously changes due to aging, thermal effects and other influences during the mission period. This has been taken into account in the analysis using the methods of LAD sensitivity calibration based on Lyman-α-bright stars and the undisturbed H geocorona (see details in Zoennchen et al., 2015, 2013) as sources of known Lyman-α flux. Nevertheless, the LADs' sensitivity can be assumed to be constant in short time periods from a few hours up to several days, which are used here to analyze exospheric Lyman-α variations during geomagnetic storms.

3 Analytic approach

With TWINS-LAD LOS observations we can study the exospheric Lyman-α radiation and its variation between 3 and 8 R_e. This radiation originates from the resonant scattering of (mostly) solar Lyman-α photons at the H atoms within the exosphere.

Following Anderson and Hord Jr. (1977), a medium with an optical depth τ on the order of 0.1 or less can be defined as optically thin since 90 % of the photons are not influenced by multiple-scattering effects. Above 3 R_e geocentric distance the low n_H values allow for the assumption of single scattering along LOSs, since they are in the optically thin regime for the Lyman-α scattering process. This implies that the exospheric Lyman-α LOS intensity is proportional to the H column density along the LOS. The equivalence is of course true for normalized, relative variations in both in [%]:

$$\Delta I_{Ly_\alpha}(\text{LOS}) = \Delta n_H(\text{LOS}). \tag{1}$$

The observational geometry of a TWINS-LAD LOS measurement can be characterized by two parameters: the spacecraft position r_{SC} and the LOS view direction s, both treated in this analysis in ECI coordinates (ECI: Earth-centered inertials with z axis towards terrestrial North Pole, x axis towards vernal equinox and x, y plane within the Earth's equator). We used the fact that after a periodic 24 h time interval ($t_1 = t_0 + 24$ h) each TWINS spacecraft is located in t_1 near to its t_0 position again ($r_{SC}(t_1) \approx r_{SC}(t_0)$) and observes practically similar LOSs in terms of the view direction $s(t_1) \approx s(t_0)$. Quantitatively, we consider two observations at t_0 and t_1 as a "pair of similar observations" if the distance in each Cartesian dimension of their TWINS positions, $r_{SC}(t_0)$ and $r_{SC}(t_0)$, is ≤ 500 km and if the angular distance for both of the spherical angles (ECI longitude and latitude) of their view directions $s(t_0)$ and $s(t_1)$ is $\leq 2°$, respectively.

In order to study the variability in the exospheric H density at t_1 with respect to t_0, we have to calculate the relative Lyman-α intensity difference of those two LOS1(t_0)/LOS2(t_2) pairs:

$$\Delta I_{Ly_\alpha}(t_1, t_0) = \frac{I_{Ly_\alpha}(\text{LOS2}(t_1)) - I_{Ly_\alpha}(\text{LOS1}(t_0))}{I_{Ly_\alpha}(\text{LOS1}(t_0))}. \tag{2}$$

Within a given observational time window (e.g., $t_w = 4$ h) a lot of "pairs of similar observations" can be collected from the two time intervals $t_0 + t_w$ and $t_1 + t_w$.
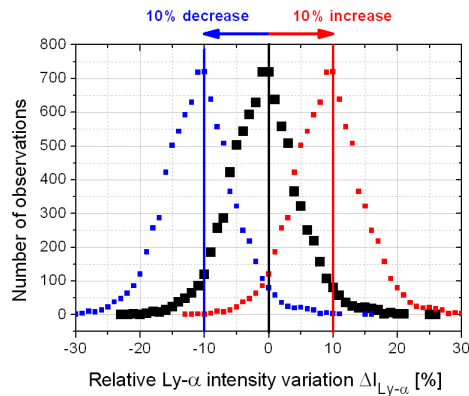
Figure 1. Black: the relative Lyman-α intensity variations from "pairs of similar observations" taken with a time shift of 24 h for 13/14 June 2008. The 0 % shift of the black Gaussian curve indicates a constant exosphere without variations in n_H. Red: schematic plot for a $+10$ % increase in n_H. Blue: schematic plot for a -10 % decrease in n_H.

Based on Eq. (2) we have calculated all those $\Delta I_{Ly_\alpha}(t_1, t_0)$ values for the two quiet days 13/14 June 2008 and plotted them in Fig. 1 (black dots). As expected, a Gaussian-like error distribution appears because of the small but existing deviations of the spacecraft positions, view directions and the count statistics for every measured Lyman-α intensity. The peak of this (black) Gaussian curve is located near 0 %, which describes the situation of nothing changing inside the exosphere between those two quiet days.

In the case of an $+10$ % increased H density, the peak of the Gaussian curve will be shifted to $+10$ % (see schematic red curve in Fig. 1). A -10 % decreased H density will consequently shift the Gaussian peak to -10 % (see schematic blue curve in Fig. 1). The [%] position of the Gaussian peak can be named as the most likely H density variation Δn_H within the chosen observational time window. Most of the further plots and arguments in this work refer to this value.

Daily variations in the total solar Lyman-α flux are very small in the analyzed periods but are nevertheless considered and removed from the LOS observations (see Sect. 5). Additional external Lyman-α components, e.g., from the interplanetary Lyman-α background or from UV-bright stars, were also subtracted before the analysis (see Sect. 4).

4   Correction for interplanetary Lyman-α background and bright UV stars

In order to correct the obtained Lyman-α signal for the interplanetary Lyman-α background, produced by the interplanetary hydrogen density distribution, we used an appropriate model. The assumption used and the model itself is described in greater detail in Zoennchen et al. (2015). The parameters of this model are adjusted such that the interplanetary Lyman-α intensities are in good agreement with maps pro-
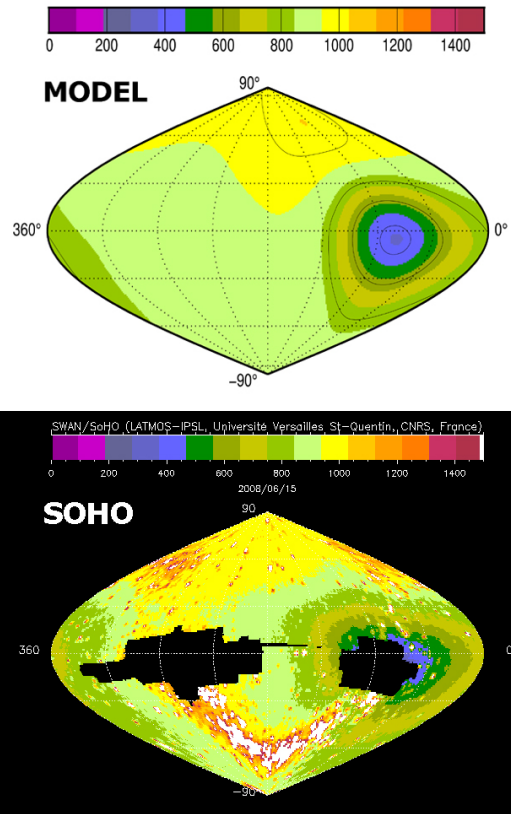

Figure 2. Solar minimum all-sky maps for interplanetary Lyman-α background intensities (R) for 15 June 2008. Top: our simulated hot-model Lyman-α intensity map using $A_N = A_S = 0.4$, $b_e = 0.04$, and $b_w = 11.5°$. Bottom: observed Lyman-α all-sky intensities by SOHO/SWAN (provided via Web by LATMOS-IPSL, Université Versailles St-Quentin, CNRS, France: http://swan.projet.latmos.ipsl.fr/images/)

vided by SOHO/SWAN (see also Bertaux et al., 1998). An example is given in Fig. 2.

Also the Lyman-α component of stars with a bright UV radiation component (e.g., young O-type stars) was removed from these contaminated LOS observations. For this purpose we created one all-sky mask (with an 8° circle around each star) to mask the 90 UV-bright stars as published in Snow et al. (2013).

5   Analyzed geomagnetic storm events

In total eight different geomagnetic storms and their influences on the exospheric H density between 3 and 8 R_e were analyzed: four storms during the solar minimum between June–August 2008, one storm in the transition between solar minimum and maximum in October 2011, and three storms near the solar maximum between June and October in 2013. This selection was also intended to investigate differences in
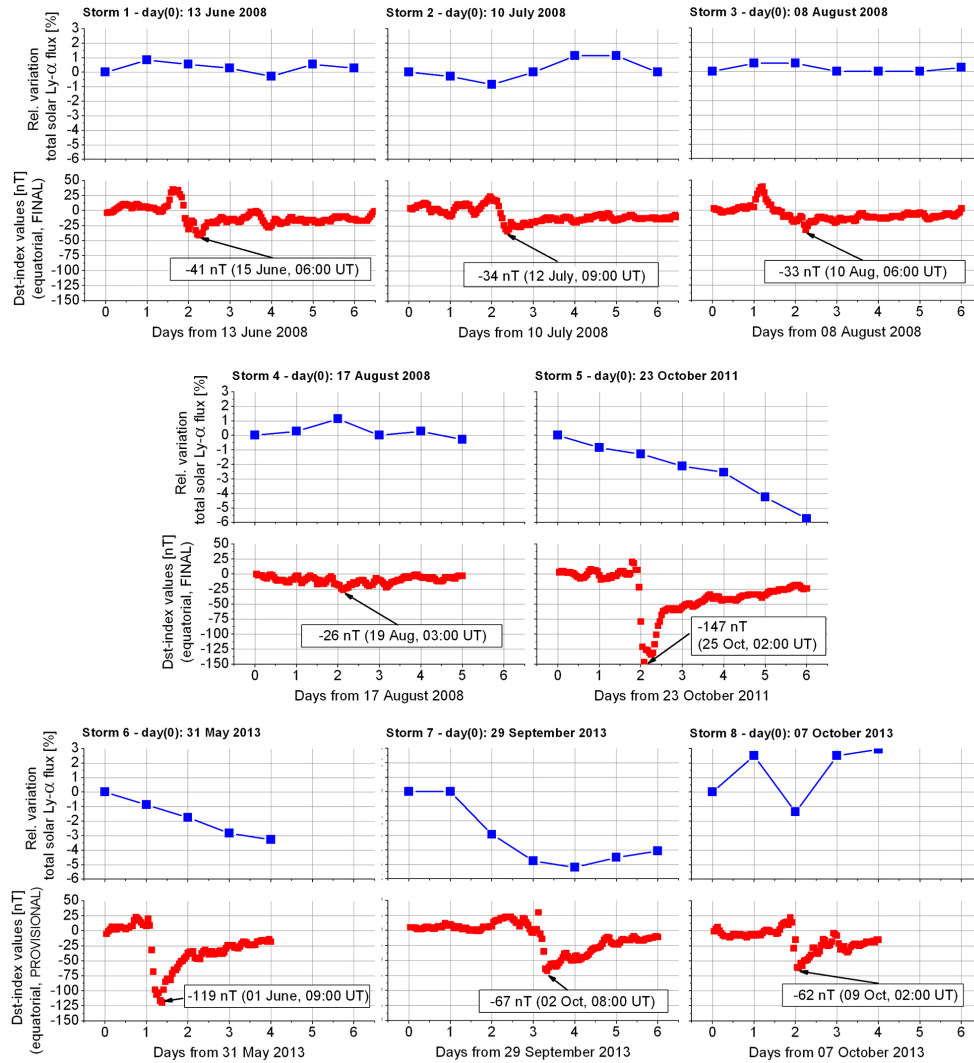
Figure 3. Plotted for each analyzed storm (1–8). Top: relative variation in the total solar Ly-α flux [%] with respect to the storm's reference day (flux values provided by LASP: http://lasp.colorado.edu/lisird) (blue). Bottom: hourly values of the Dst index (equatorial) (nT) (provided by the WDC for Geomagnetism, Kyoto: http://wdc.kugi.kyoto-u.ac.jp/wdc/Sec3.html) (red).

the exospheric reaction under solar minimum and maximum conditions.

Between June–August 2008 the LADs of both TWINS1/2 spacecraft observed simultaneously under very stable operational conditions with optimal spatial and temporal coverage. Therefore, all solar minimum storms within the sample were taken from that period. Near solar maximum the number of LAD data is significantly reduced, since LAD data are then available from TWINS1 only. Additionally, all LOSs with angles $\leq 90°$ with respect to the Sun were removed because of Lyman-α-stray light. In particular the three analyzed storms near solar maximum in 2013 were observed by the TWINS1 LADs with an acceptable observational coverage.

Table 1 shows each storm event with start date, the Dst peak value and the Kp index daily sum. According to standard classification, the observed storms are of type "weak" and "moderate" (from -26 to -147 nT) with respect to their peak Dst indices.

In Fig. 3 (top, blue squares) the variation in the daily total solar Lyman-α flux [%] with respect to a reference day short before the storm is presented for each storm. The flux values were measured by the Solar EUV Experiment (SEE) of the TIMED/SEE satellite, the SORCE SOLar Stellar Irradiance Comparison Experiment (SOLSTICE) aboard the UARS satellite and the Extreme Ultraviolet Variability Experiment (EVE) aboard the SDO spacecraft, calibrated to the UARS SOLSTICE level (see, e.g., Woods et al., 2000) and provided by LASP (http://lasp.colorado.edu/lisird).

It is clear from Fig. 3 that there are the small variations in the daily total solar Lyman-α flux, in particular ≤ 1 % during

Table 1. Analyzed geomagnetic storm events between 2008 and 2013 and their characteristic geomagnetic index values.

Storm no.	Date (yyyy-mm-dd)	Strength	Peak Dst index (nT)	Kp index daily sum (nT)
1	2008-06-15	weak	−41	250
2	2008-07-12	weak	−34	240
3	2008-08-09	weak	−33	260
4	2008-08-18	weak	−26	263
5	2011-10-25	moderate+	−147	277
6	2013-06-01	moderate	−119	397
7	2013-10-02	moderate	−67	390
8	2013-10-09	moderate	−62	303

the solar minimum. Nevertheless, the TWINS LOS data are corrected for these variations by normalization of all LAD observations to the total solar Lyman-α flux of a fixed reference day (see Zoennchen et al., 2015).

Additionally, Fig. 3 (bottom, red) shows the timeline of the Dst index values during each storm (hourly and equatorial, provided by the WDC for Geomagnetism, Kyoto: http://wdc.kugi.kyoto-u.ac.jp/wdc/Sec3.html) to illustrate the actual geomagnetic conditions.

The duration of the storms is between 1 and 4 days, which is best visible from the relaxation of the Kp index daily sum in Fig. 4. In particular the storms during solar minimum show a slow recovery behavior of several days.

6 Increase in the neutral H column density

The analysis of the (carefully cleaned) TWINS LAD LOS observations from all eight different geomagnetic storms shows one result very clearly: in every single case the exosphere above 3–8 R_e responded to the geomagnetic disturbance with an increase in the resonantly scattered Lyman-α intensity $\Delta I_{Ly-\alpha}$ [%]. That corresponds to an increase in the neutral H column density Δn_H [%] by the same amount, since the LOSs are completely within the optically thin regime above 3 R_e.

The maximal Δn_H peak value during the storms was found to be between 9 and 23 % with respect to a quiet reference day shortly before the storm (see Table 2). Interestingly, the very weak storms 1, 2 and 3 under solar minimum conditions are among those with the largest Δn_H peak values up to 23 %. With the analyzed storm sample in this work, we found that there is a tendency towards a decreasing relative exospheric H density reaction to an increasing storm intensity. Nevertheless, a simple linear correlation between the Δn_H peak value and one of the two geomagnetic indices (peak value Dst index and Kp index daily sum) does not seem to exist (for both indices, see Sect. 8).

Figure 4 shows the timeline of the relative H column density increase Δn_H during each storm. The time resolution t_{res} is varying and depends on the availability of LOS observa-

Table 2. Peak values of the exospheric Lyman-α intensity variation $\Delta I_{Ly-\alpha}$ (here equal to H column density variation Δn_H) and the time delay between the moment when the first significant dynamic solar wind pressure peak (p_{SW}) hits the Earth and the moment when $\Delta I_{Ly-\alpha}$ reaches its maximum.

Storm no.	Date (yyyy-mm-dd)	Peak letter	$\Delta I_{Ly-\alpha}$ [%]	Δt_{delay} (h)
1	2008-06-15	A	20.3	13
2	2008-07-12	A	23.4	14
3	2008-08-09	A	5.5	11
3	2008-08-09	B	17.4	12
4	2008-08-18	A	9.5	11
4	2008-08-18	B	9.1	12
5	2011-10-25	A	10.5	11
6	2013-06-01	A	13.2	13
7	2013-10-02	A	11.9	9
8	2013-10-09	A	18.7	11

tions from one or both TWINS spacecraft at each time. Additionally, Fig. 4 shows the Kp index daily sum values in order to illustrate that the Δn_H increases and the global geomagnetic disturbance recovers over time on a very similar timescale after the maximum (see Sect. 7).

Further interesting timing effects were found: The exosphere seems to react immediately with a density increase after the first significant increase in the dynamic solar wind pressure p_{SW} hits the Earth – hours before the Dst index peak. But nevertheless, the exosphere reaches its maximum Δn_H value after a 9–14 h time shift to the first p_{SW} peak (for both effects see also Sect. 7).

The total uncertainties are expected as the sum of the uncertainty in the background-corrected Lyman-α intensities of about ≈ 10–15 % (as discussed in Zoennchen et al., 2015) and the uncertainty in the Gaussian fit, which was found to be ≈ 2–5 %. Therefore, in total we expect uncertainties of ≈ 12–20 %.
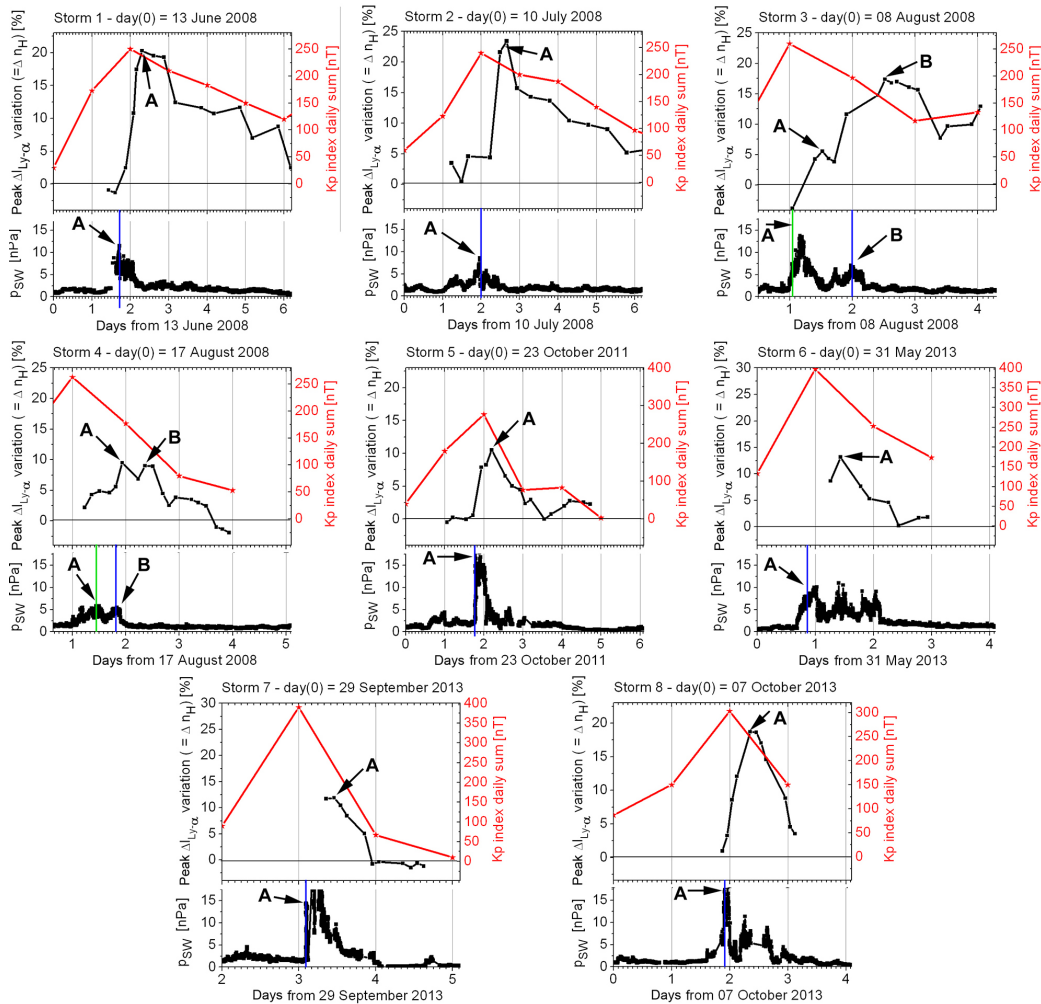
Figure 4. Plotted for each analyzed storm (1–8). Top: the relative increase in the exospheric Lyman-α intensity $\Delta I_{Ly-\alpha}$ [%] (here equal to H column density increase Δn_H) with respect to the storm's reference day (black) and the Kp index daily sum (nT) (red) (provided by the UK Solar System Data Center: http://www.ukssdc.ac.uk/wdcc1/data_menu.html). Bottom: the dynamic solar wind pressure p_{SW} (nPa) near the Earth (taken from ACE observations and published on the CDA website of NASA Goddard Space Flight Center: http://cdaweb.sci.gsfc.nasa.gov/index.html). Corresponding pairs of (p_{SW}, $\Delta I_{Ly-\alpha}$) peaks are labeled with A and B.

7   Time delay of the geocoronal H density reaction

The analyzed eight geomagnetic storms always started with a rapid increase in the dynamic solar wind pressure (p_{SW}). Those pressure increases cause a compression of the terrestrial magnetosphere and deposit thermal energy into the lower exosphere. If the pressure increase is significant enough, the resulting increase in the exospheric temperature might trigger effective transport mechanisms of H atoms from lower to upper regions. We found that this is the case for pressure increase events of $p_{SW} > 7$–10 [nPa].

This leads to a density increase in the upper regions that we have observed with TWINS LAD between 3 and 8 R_e geocentric distances.

As one result we found that there is a time shift of about 9–14 h (most likely 11–12 h) between the moment when the

first significant increase in p_{SW} hits the Earth and the moment when the maximum Δn_H peak can be detected as the exospheric response to the storm event (see Table 2 for all time shift values Δt_{delay}).

On the other hand, the H column density immediately starts its continuous increase from 0 to the maximum Δn_H peak [%] after the associated p_{SW} peak hits the Earth – mostly several hours before the Dst index reaches its negative peak.

In the case of multiple p_{SW} peaks during one storm, a multiple Δn_H peak signature is also often derivable from the TWINS-LAD data when the time resolution is good enough (e.g., see storms 3 and 4 in Fig. 5; corresponding peaks are labeled with A and B).
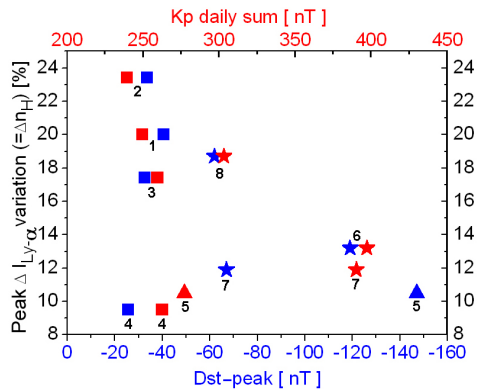
Figure 5. Between 3 and 8 R_{e} the peak values of the relative exospheric Lyman-α intensity variation $\Delta I_{\mathrm{Ly\text{-}\alpha}}$ (here equal to the LOS H column density variation Δn_{H}) show the tendency to decrease with increasing peak value of the Dst index (nT) (blue) or the Kp index daily sum (nT) (red), but there is no obvious linear correlation between them (in particular not for the weaker storms with Dst peak $> -70\,\mathrm{nT}$). Symbols: squares, storms at solar minimum; triangles, storms in the transition period between solar minimum and maximum; stars, storms near solar maximum. Numbers indicate the storm event number from Table 1.

For the weak storms 1 and 2 during the quiet phase of the very low solar minimum in 2008, the time shift, of 13–14 h, tends to be a little bit larger than the average time shift of $\approx 11\,\mathrm{h}$ from all other storms. More storms need to be analyzed in order to answer the question of whether this is a real phenomenon or just statistics.

8 Correlation of the exospheric variation with characteristic storm indices

For each of the eight analyzed geomagnetic storms, the resulting maximum relative H column density increase Δn_{H} [%] as the exospheric response between 3 and 8 R_{e} can be seen in Fig. 4 and Tab. 2. In the case of the storms 3 and 4, we could identify two maxima (labeled as A and B in Fig. 4) on different days caused by two separate p_{SW} peaks.

Interestingly, the relative exospheric H density reactions to the analyzed storms show the tendency to decrease with increasing storm intensity (e.g., peak values Dst index). Nevertheless, the Δn_{H} peaks do not seem to be derivable from the peak value of the Dst index or the Kp index daily sum using a simple linear correlation function (see Fig. 5). We found that (in particular weak) storms with very similar peak values of the Dst index and Kp index daily sum can have very different Δn_{H} peak values.

From these results we can conclude that the value of the Δn_{H} peak is not linearly controlled by the values of the two mentioned geomagnetic indices during storms. It seems to be more likely that a combination of different and/or additional parameters is necessary in order to better predict the H col-

umn density reaction of the H geocorona. This might include characteristic numbers of the solar wind and parameters of the actual exospheric H density distribution. In particular, the density level of the H geocorona itself, which strongly depends from the current solar activity conditions (and is therefore influenced by long- and short-term variations), can be an important parameter to explain different geocoronal H density reactions during comparable storms.

The linear correlation between Δn_{H} and Dst index peak values as published by Bailey and Gruntman (2013) taken from storms in 2011 could therefore not be confirmed in this analysis, which includes storms from the solar minimum period in 2008 and the solar maximum 2013.

The presented results also show that very weak geomagnetic storms during solar minimum can cause large Δn_{H} peaks (up to 23 %) compared to moderate storms in periods with a significant higher solar activity. A possible reason for that phenomenon might be an overall lower H density level in the undisturbed exosphere at solar minimum compared to solar maximum (Zoennchen et al., 2015). Within a thinner exosphere, the same number of H atoms transported from lower to larger distances will create a higher-percentage Δn_{H} peak value.

9 Conclusions

Based on TWINS-LAD LOS observations, temporal variations in the resonant scattered Lyman-α radiation ($\Delta I_{\mathrm{Ly\text{-}\alpha}}$) from the exosphere between 3 and 8 R_{e} (geocentric distance) were studied during eight different geomagnetic storm events (peak Dst index -26 to $-147\,\mathrm{nT}$).

Above 3 R_{e}, variations in the exospheric $\Delta I_{\mathrm{Ly\text{-}\alpha}}$ are interpretable as equivalent H column density variations (Δn_{H}) along the LOS, since the LOSs are completely situated within the optically thin region. Other Lyman-α sources than the exospheric component (e.g., interplanetary background, bright UV stars) were consequently removed before the analysis. Additionally, temporal variations in the daily total solar Lyman-α flux as illumination input for the resonant scattering process in the exosphere were corrected by the normalization of the LOS observations to the solar flux of a fixed reference day.

For all storms an increase in the H column density Δn_{H} (range: 9–23 %) was found as exospheric reaction between 3 and 8 R_{e}. Interestingly, we found in particular that very weak storms under solar minimum conditions are among those with the largest relative H column density increases (up to 23 %) in our storm sample (see, e.g., storm no. 1, 2 and 3). Since we observe with the most distant LOSs of TWINS LAD not too far from the transition zone between terrestrial exosphere and unbound interplanetary medium, the results suggest that the escape flux of H atoms might be increased by a very similar relative amount, too. Thermal (and possibly nonthermal) transport processes of H atoms, which are

triggered by geomagnetic storms, seem to be responsible for the observed redistribution of H density from lower to upper regions within the exosphere.

The exospheric H density reactions relative to the analyzed storms show the tendency to decrease with increasing storm intensity (e.g., peak values Dst index). Nevertheless, a simple linear correlation between the peak value Dst index (or the Kp index daily sum) of a storm and the maximal relative increase in the exospheric H column density does not seem to exist for the analyzed distances and storms. In contrast to this, we found for several storms with very similar peak Dst values very different exospheric Δn_H reactions (e.g., between 9 and 23 %). This implies that more and possibly other parameters (e.g., of the solar wind and/or of the exospheric H density distribution itself) are needed in order to be able to better predict the exospheric maximum Δn_H reaction caused by geomagnetic storms.

From the analysis we additionally found that the maximal relative Δn_H increase followed by a time delay between 9 and 14 h after the first significant increase in the dynamic solar wind pressure (p_{SW}) hits the Earth. Moreover, the exosphere reacts nearly immediately after the first p_{SW} peak with a continuous density increase. After reaching the maximum density, the amount of the geomagnetic disturbance (Kp index daily sum) and the density increase are recovering on very similar timescales. This was found for storms with both slow recovery ($\approx$ 4 days) and faster recovery ($\approx$ 1–1.5 days).

10   Data availability

TWINS-LAD data are available at the NASA CDAWeb (see http://cdaweb.sci.gsfc.nasa.gov/index.html). TWINS images are available from the TWINS website of the Southwest Research Institute (SWRI) in San Antonio, Texas, USA (see http://twins.swri.edu/).

References

Anderson, D. E. and Hord Jr., C. W.: Multidimensional radiative transfer – Applications to planetary coronae, Planet. Space Sci., 25, 563–571, doi:10.1016/0032-0633(77)90063-0, 1977.

Bailey, J. and Gruntman, M.: Observations of exosphere variations during geomagnetic storms, Geophys. Res. Lett., 40, 1907–1911, doi:10.1002/grl.50443, 2013.

Bertaux, J. L., Pellinen, R., Chassefiere, E., Dimarellis, E., Goutail, F., Holzer, T. E., Kelha, V., Korpela, S., Kyrölä, E., and Lallement, R.: SWAN: A study of solar wind anisotropies, in: ESA, The SOHO Mission, Scientific and Technical Aspects of the Instruments, 63–68, 1998.

Bishop, J.: Analytic exosphere models for geocoronal application, Planet. Space Sci., 39, 885–893, 1991.

Carruthers, G. R., Page, T., and Meier, R. R.: Apollo 16 Lyman alpha imagery of the hydrogen geocorona, J. Geophys. Res., 81, 1664–1672, 1976.

Chamberlain, J. W.: Planetary coronae and atmospheric evaporation, Planet Space Sci., 11, 901–960, 1963.

Fahr, H. J. and Shizgal, B.: Modern Exospheric Theories and Their Observational Relevance, Rev. Geophys. Space Phys., 21, 75–124, 1983.

Hodges Jr., R. R.: Monte Carlo simulation of the terrestrial hydrogen exosphere, J. Geophys. Res., 99, 23229–23247, 1994.

Johnson, F. S.: The Distribution of Hydrogen in the Telluric Hydrogen Corona, Astrophys. J., 133, 701–705, doi:10.1086/147072, 1961.

Kupperian, J. E., Byram, E. T., Chubb, T. A., and Friedman, H.: Far ultra-violet radiation in the night sky, Planet. Space Sci., 1, 3–6, doi:10.1016/0032-0633(59)90015-7, 1959.

McComas, D. J., Allegrini, F., Baldonado, J., Blake, B., Brandt, P. C., Burch, J., Clemmons, J., Crain, W., Delapp, D., Demajistre, R., Everett, D., Fahr, H., Friesen, L., Funsten, H., Goldstein, J., Gruntman, M., Harbaugh, R., Harper, R., Henkel, H., Holmlund, C., Lay, G., Mabry, D., Mitchell, D., Nass, U., Pollock, C., Pope, S., Reno, M., Ritzau, S., Roelof, E., Scime, E., Sivjee, M., Skoug, R., Sotirelis, T. S., Thomsen, M., Urdiales, C., Valek, P., Viherkanto, K., Weidner, S., Ylikorpi, T., Young, M., and Zoennchen, J.: The Two Wide-angle Imaging Neutral-atom Spectrometers (TWINS) NASA Mission-of-Opportunity, Space Sci. Rev., 142, 157–231, doi:10.1007/s11214-008-9467-4, 2009.

Nass, H. U., Zoennchen, J. H., Lay, G., and Fahr, H. J.: The TWINS-LAD mission: Observations of terrestrial Lyman-α fluxes, Astrophys. Space Sci. Trans., 2, 27–31, doi:10.5194/astra-2-27-2006, 2006.

Østgaard, N., Mende, S. B., Frey, H. U., Gladstone, G. R., and Lauche, H.: Neutral hydrogen density profiles derived from geocoronal imaging, J. Geophys. Res.-Space, 108, 1–12, doi:10.1029/2002JA009749, 2003.

Rairden, R. L., Frank, L. A., and Craven, J. D.: Geocoronal imaging with Dynamics Explorer, J. Geophys. Res., 91, 13613–13630, 1986.

Snow, M., Reberac, A., Quémerais, E., Clarke, J., McClintock, W. E., and Woods, T. N.: A New Catalog of Ultraviolet Stellar Spectra for Calibration, Cross-Calibration of Far UV Spectra of Solar System Objects and the Heliosphere, ISSI Scientific Report Series, Vol. 13, ISBN 978-1-4614-6383-2, Springer Science & Business Media New York, 191–226, 2013.

Thomas, G. E. and Bohlin, R. C.: Lyman-alpha measurements of neutral hydrogen in the outer geocorona and in interplanetary space, J. Geophys. Res., 77, 2752–2761, 1972.

Woods, T. N., Tobiska, W. K., Rottman, G. J., and Worden, J. R.: Improved solar Lyman alpha irradiance modeling from 1947 through 1999 based on UARS observations, J. Geophys. Res., 105, 27195–27215, doi:10.1029/2000JA000051, 2000.

Zoennchen, J. H., Nass, U., and Fahr, H. J.: Exospheric hydrogen density distributions for equinox and summer solstice observed with TWINS1/2 during solar minimum, Ann. Geophys., 31, 513–527, doi:10.5194/angeo-31-513-2013, 2013.

Zoennchen, J. H., Nass, U., and Fahr, H. J.: Terrestrial exospheric hydrogen density distributions under solar minimum and solar maximum conditions observed by the TWINS stereo mission, Ann. Geophys., 33, 413–426, doi:10.5194/angeo-33-413-2015, 2015.